

# Triple-shape memory effect in a styrene-based shape memory polymer: Characterization, theory and application

Haiyang Du<sup>1</sup>, Liwu Liu<sup>1</sup>, Fenghua Zhang<sup>2</sup>, Jinsong Leng<sup>2,\*</sup>, Yanju Liu<sup>1,\*\*</sup>

<sup>1</sup> Department of Astronautical Science and Mechanics, Harbin Institute of Technology, Harbin, 150001, People's Republic of China

<sup>2</sup> National Key Laboratory of Science and Technology on Advanced Composites in Special Environments, Harbin Institute of Technology, Harbin, 150080, People's Republic of China

## ARTICLE INFO

### Keywords:

Shape memory polymer  
Triple-shape memory effect  
FEM simulation  
Polymer application

## ABSTRACT

A segmented styrene-based shape memory polymer (SMP) comprising two types of SMP materials (S1-SMP and S2-SMP) was fabricated by using a two-step curing method to exhibit the triple shape memory effect (triple-SME). The material properties of S1-SMP and S2-SMP parts were explored using dynamic mechanical analysis, multi-frequency scan testing, thermal expansion measurements, static tensile testing and shape memory testing, respectively. Meanwhile, the triple-SME of segmented SMP was also characterized by shape memory testing with continue heating step. These experimentally determined material properties were incorporated into the theoretical model for the triple-SME based on a phase transition model and Generalized Maxwell model. Experimental verification was obtained by observing the triple-SME behavior under uniaxial tensile strain of 20%. Finally, the triple-SME behavior of SMP was assessed in two engineered implementations; a programmable self-deployed structure model and double bottle-shaped smart mandrel. Good agreement was demonstrated between experimental result and a finite-element model (FEM) simulation during the continue heating recovery step.

## 1. Introduction

As an important member of a generic class of stimulus-responsive polymers, shape memory polymers (SMPs) have the ability to maintain one or more temporary shapes and subsequently recover the initial shape when subjected to external stimuli, such as temperature, electricity, light, magnetic field and solution [1–6]. Since SMP was developed in 1990s, researchers from every corner of the world have paid more and more attention to SMPs and their composites (SMPCs), including synthesis processes [7], thermo-mechanical properties [8], actuation methods [9] and constitutive models [10–12]. Compared to shape memory alloys and shape memory ceramics, SMPs have the advantage of low cost, high shape deformation and recovery ability, good biocompatibility and biodegradability, and wide transition temperature range [1–3]. Nowadays, SMPs and SMPCs are widely used in aerospace [13], biomedicine [14], and textiles [15], information carriers [16] and smart sensors [17].

Dual-shape memory polymers (dual-SMPs) are only able to remember one temporary shape. However, triple-shape memory polymers (triple-SMPs) and multi-shape memory polymers (multi-SMPs) can

remember two or more temporary shapes in a thermo-mechanical cycle, leading to their potential for realization of complex movements and functions (e.g. in smart actuators, smart sensors and the like). Commonly, triple-SMPs can be divided into single-, and multi-stimulus types based on the actuation method. Furthermore, single-stimulus SMPs can be further divided into those with two well-separated transition temperatures and those with a broad transition temperature.

Single-stimulus triple-SMPs with two well-separated transition temperatures were first reported by Lendlein et al., in 2006 [18,19], based on tailoring composition ratios to form two segregated domains in molecular structure with significantly different phase transition temperature (glass transition temperature ( $T_g$ ) or melt temperature ( $T_m$ )). Pretsch et al. synthesized a kind of poly(ester urethane) with triple-SME properties based on two well-separated  $T_g$  and  $T_m$ , and characterized the shape fixity/recovery abilities and aging properties [20,21]. Hu et al. firstly prepared a triple-SMPU with two different  $T_m$ s [22]. Xin et al. prepared a Eucommia rubber/polyethylene SMPC by simple physical blending to form a material with triple-SME properties with two  $T_m$ s [23]. In addition, triple-SME properties have also been achieved with bilayer structures. Xie et al. (2009) realized the triple-SME by

\* Corresponding author.

\*\* Corresponding author.

E-mail addresses: [lengjs@hit.edu.cn](mailto:lengjs@hit.edu.cn) (J. Leng), [yj\\_liu@hit.edu.cn](mailto:yj_liu@hit.edu.cn) (Y. Liu).

developing a bilayer structure made of two types of epoxy-based dual-SMP with well-separated transition temperatures between 20 °C and 89 °C [24,25]. Kim et al. mixed different weight ratio silica nanocomposites into a SMPU matrix to form two films with different  $T_g$ s and prepared a bilayer structure possessing good triple-SME [26]. Using a similar approach, Bowman et al. prepared a bilayer structure possessing triple-SME using thiol-X chemistries with different  $T_g$ s [27].

A single-stimulus triple-SMP with a broad transition temperature was reported by Huang et al., in 2005 in a SMPU that can program recovery shapes to realize triple/multi-SME by varying the immersion time in water [28,29]. Zhou et al. synthesized a SMPU with a transition temperature from 25 °C to 75 °C by adjusting the weight ratio of two compositions and demonstrated excellent triple-SME properties using temperature and water actuation [30]. Xie et al. demonstrated the dual-, triple- and multi-shape memory effect of Nafion film over a wide glass transition zone (from 55 °C to 130 °C) [31,32]. In addition, Zhang et al. demonstrated the triple- and multi-SME properties of a fibrous Nafion membrane that had been prepared using an electrospinning method [33]. Leng et al. synthesized a thermosetting bismaleimide-based triple-SMP with a high transition temperature zone from 80 °C to 160 °C for future smart aerospace structures [34]. Wang et al. prepared a thermoplastic polyimide-based SMP by adjusting the weight ratios of benzoxazole to achieve a wide transition temperature from 230 °C to 350 °C that can meet the requirements of a high temperature actuator [35].

Multi-stimulus triple-SMPs have been reported by several authors. Lendlein et al. added silica coated magnetic sensitive nanocomposite ( $Fe_3O_4$ ) to a PCL-based SMP and realized triple-SME by increasing the magnetic field strength from 0 kA/m to 30 kA/m at a frequency of 258 kHz [36]. Xie et al. fabricated a multi-SMP by adding  $Fe_3O_4$  and carbon nanotubes (CNT) into two different regions of an epoxy matrix to demonstrate the shape recovery process of two regions by using elective radiofrequencies at different regions (30 kHz for  $Fe_3O_4$  region and 13.56 MHz for CNT region) [37]. Leng et al. synthesized a styrene-based triple-SMP and prepared a composite with three regions: SMP matrix filled with  $Fe_3O_4$ (region 1), neat SMP (region 2), and SMP matrix filled with CNT (region 3). The triple-SME for regions 1 and 3 was achieved using radiofrequency activation at frequencies of 30 kHz and 13.56 MHz, respectively [38]. Hu et al. prepared an epoxy-based multi-region SMP consisting of neat epoxy region and a region with embedded UV-sensitive materials and demonstrated triple-SME using sequential UV activation and heat actuation [39]. Yu et al. developed a selective-wavelength photo-responsive epoxy-based SMP composite and demonstrated the triple-, multi-SME by adjusting the activation wavelength between 365 nm and 800 nm [40].

Up to now, investigation of the thermo-mechanical behavior of triple-SMPs has mostly focused on experimentation and there are only a few literature that provide a theoretical understanding. Huang et al. proposed a framework including an elastic and reversible transition phase in parallel to explain the triple-, multi-SME of polymers by freezing and activating the reversible transition phase with changing temperature [41]. In 2012, Yu et al. firstly developed a multi-branch Generalized Maxwell model to characterize triple-SME of Nafion film [42]. According to Yu's work, Arrieta et al. imported the Generalized Maxwell model with 20-branches and WLF equation into finite element software ABAQUS and simulated the triple-SME of a SMP with a two-step temperature recovery process [43]. However, the theoretical models were typically used to demonstrate the triple-SME of SMPs under stage heating recovery step, sometimes the triple-SME would disappear under continue heating step.

In our work, a segmented-SMP with triple-SME was prepared using a two-step curing method based on two types of styrene-based SMPs (S1-SMP and S2-SMP) with well-separated  $T_g$ . The thermo-mechanical properties of S1-SMP/S2-SMP were characterized and dual-/triple-SME behavior was demonstrated. Two types of constitutive models based on the Liu model and Generalized Maxwell model were

investigated to gain a theoretical insight and good agreement with experimental results was seen for triple-SMP under uniaxial tension deformation. Finally, the triple-SME behavior was assessed and verified in two engineered implementations; a programmable self-deployed structure model and a double bottle-shaped smart mandrel. Good shape recovery behavior was observed in these implementations.

## 2. Materials and experiments

**Materials and preparation** Based on previous work [44], two types of styrene-based SMPs with well-separated  $T_g$  were synthesized by adjusting the weight ratio between the styrene monomer and the cross-linking agent. The SMP with higher  $T_g$  was designated "S1-SMP" and the other was "S2-SMP". A styrene-based triple-SMP was prepared using a two-step curing method. First, S1-SMP was poured into a mold made of glass slides with a spacing of 2.8 mm and cured for 1 h. Then, S2-SMP was added on top of S1-SMP and fully cured in an oven at 75 °C for 24 h. The cured segmented triple-SMP plate was cut into rectangular and dumbbell-shaped samples for dynamic mechanical analysis, static tensile testing and shape memory testing.

**Dynamic mechanical analysis (DMA) test** The  $T_g$ s of S1-SMP/S2-SMP were measured using a dynamic mechanical analyzer (DMA Q800, TA Instruments, USA). Samples taken from the S1-SMP and S2-SMP regions of the cured segmented plate were cut into rectangular strips with dimensions 30 mm × 5 mm × 2.8 mm (length × width × thickness).  $T_g$  was determined by tensile mode at a frequency of 1 Hz with a deformation amplitude of 0.015 mm. The temperature scan range was 25 °C–120 °C with a heating rate of 1 °C/min. As with our previous work [45,46],  $T_g$  was taken to be the temperature at which the derivative of the storage modulus reached its maximum value. The values were 62 °C and 43 °C for S1-SMP and S2-SMP respectively.

**Multi-frequency scan test** Multi-frequency scan testing of S1-SMP/S2-SMP was also carried out by DMA Q800 to characterize the relationship between storage modulus and dynamic frequency at different temperatures. Deformation amplitude of 0.010 mm was used and the frequency range was 0.1 Hz–100 Hz. Scanning was conducted at 5 °C intervals and the temperature ranges were 30 °C–100 °C for S1-SMP and 20 °C–85 °C for S2-SMP. The sample size was identical to the DMA test. The detailed experimental process for S1-SMP was as follows: Firstly, sample was heated to 30 °C and held constant for 5 min, following which the sample was dynamically scanned from 0.1 Hz to 100 Hz. The process was then repeated for all subsequent temperature points up to the final temperature 100 °C.

**Thermal expansion measurement** The thermal expansion coefficients ( $\alpha$ ) of S1-SMP and S2-SMP were established using DMA Q800. Sample sizes were the same as DMA test, and a small load (0.001 N) was applied throughout to keep the sample under tension and maintain a straight orientation. The experimental process was as follows: the sample was heated from 25 °C to 100 °C at a rate of 2.5 °C/min, and held for 20 min to achieve thermal equilibrium, and then cooled to 25 °C at the same rate to complete a free thermal strain cycle. The sample was taken through three such thermal cycles. The thermal expansion coefficient was temperature dependent and it was determined from the ratio of the thermal strain.

**Static tensile test** The elastic moduli of S1-SMP and S2-SMP were determined using a Zwick010 (Zwick/Roell, Germany) universal tensile machine with an environmental chamber to predict the effective elastic modulus of SMP. Dumbbell-shaped samples with dimensions 115 mm × 5.8 mm × 2.8 mm (length × width × thickness) were taken from the S1-SMP/S2-SMP regions of the cured segmented SMP plate, respectively. The experimental process and measurement results were same to our previous work [45,46]. The temperature range was through  $T_g$  with increments of 10 °C, and four samples were measured under every isothermal condition for two types of SMPs.

**Shape memory test** The dual-SME of S1-SMP/S2-SMP was evaluated by conducting a tensile test using the same Zwick010 equipment.

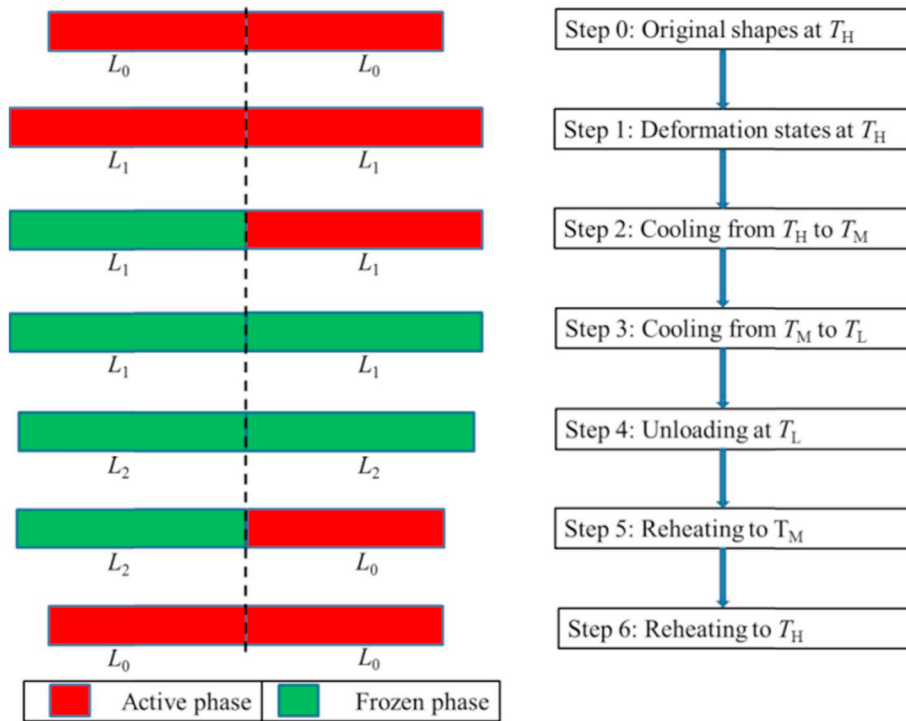


Fig. 1. Schematic of triple-shape memory process for segmented-SMP.

Taking S1-SMP as an example, the process included the following steps. Step 1: Heating S1-SMP to 70 °C and stretching by 50% at a rate of 2 mm/min. Step 2: Cooling to 30 °C at a rate of 2.5 °C/min. Step 3: Maintaining the temperature at 30 °C and removing the load to evaluate the shape fixity ability. Step 4: Reheating to the recovery temperature at 90 °C to evaluate the shape recovery ability. The same process was used to test S2-SMP. In addition, the triple-SME of the segmented-SMP was also evaluated. In this case the shape programming was conducted using a manual process and the shape recovery was conducted using a Zwick010 machine, as shown in Fig. 1. Step 1: Heating of the segmented-SMP to high temperature ( $T_H = 90$  °C) and manual stretching by 20% of the S1-SMP and S2-SMP parts at the two ends of the sample respectively. Step 2: Cooling to a middle temperature ( $T_M = 60$  °C) and freezing of S1-SMP. Step 3: Continuing cooling to a low temperature ( $T_L = 30$  °C) and freezing of S2-SMP. Step 4: Removal of the segmented-SMP load at  $T_L$ . Step 5: Reheating to  $T_M$  and activation of S2-SMP. Step 6: Continuing reheating to  $T_H$  and activation of S1-SMP. It was noted that the interface between the two types of SMPs remained fixed during the deformation and recovery process.

### 3. Constitutive models for triple-SMP

**Two-phase model** Liu et al. firstly proposed that a SMP consisted of both an active phase and a frozen phase and developed a SMP model in 2006 [11]. In our work, this theory was applied to study the triple-SME of the segmented-SMP. When cooled from  $T_H$  to  $T_M$ , the S1-SMP part of the segmented-SMP was gradually transitioned from the active state to the frozen state, however, the S2-SMP part remained in the active state due to the lower  $T_g$ . Continuing to reduce from  $T_M$  to  $T_L$ , the S2-SMP part was also gradually frozen. During the recovery step, the reverse recovery process was demonstrated with increasing temperature from  $T_L$  to  $T_H$ . The effective elastic modulus  $E_e(T)$  and frozen factor  $\phi_f$  of the SMP were fitted based on the Liu model to predict the storage strain  $\epsilon_s$  of S1-SMP/S2-SMP as follows [11].

$$E_e(T) = \frac{1}{\frac{1}{C_1} + \frac{1-\phi_f}{C_2 T}} \quad (1)$$

$$\phi_f = 1 - \frac{1}{1 + C_3(T_H - T)^n} \quad (2)$$

where,  $C_1, C_2, C_3, n$  are four material parameters whose values differ for S1-SMP and S2-SMP.

In addition, the Aydin model was also used to fit the frozen factor of S1-SMP/S2-SMP based on the literature [47] as follows.

$$\phi_f = \frac{1}{1 + \exp(b(T/T_r - (1 + \alpha)))} \quad (3)$$

where,  $a, b$  are two material parameters, and  $T_r$  is the reference temperature. These parameters were also different for S1-SMP and S2-SMP.

Furthermore, thermal expansion coefficient was also expressed based on Liu model [11].

$$\alpha = C_4 + C_5 T \quad (4)$$

where,  $C_4, C_5$  are two material parameters that differ for S1-SMP and S2-SMP.

Assuming that the initial length and deformation of the S1-SMP and S2-SMP parts in the segmented SMP were identical, then the release of storage strain with increasing temperature for the S1-SMP/S2-SMP regions can be modeled by the following equation.

$$\epsilon = \frac{\epsilon_{s1} + \int_{T_H}^T \alpha_1 dT + \epsilon_{s2} + \int_{T_H}^T \alpha_2 dT}{2} \quad (5)$$

where,  $\epsilon$  and  $T$  are the instantaneous strain and temperature of the segmented SMP during the shape recovery step, and  $\epsilon_{s1}/\epsilon_{s2}$  and  $\alpha_1/\alpha_2$  are the storage strain and thermal expansion coefficient of the S1/S2 SMPs respectively.

**Generalized Maxwell model** Based on the dual- and triple-SME research work of Yu [42,48] and Arrieta [43], multi-frequency scan testing under different temperatures was carried out to obtain storage modulus master curves at a reference temperature ( $T_C$ ). Using relative shift factors ( $\alpha_T$ ), the multi-frequency scan of storage modulus from 0.1 Hz to 100 Hz could form master curve within a more widely

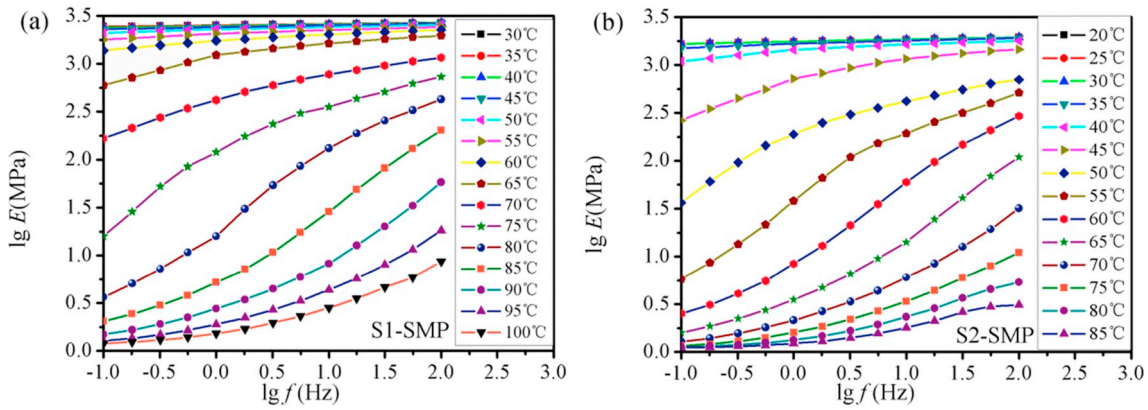


Fig. 2. Multi-frequency scan test of S1-SMP and S2-SMP.

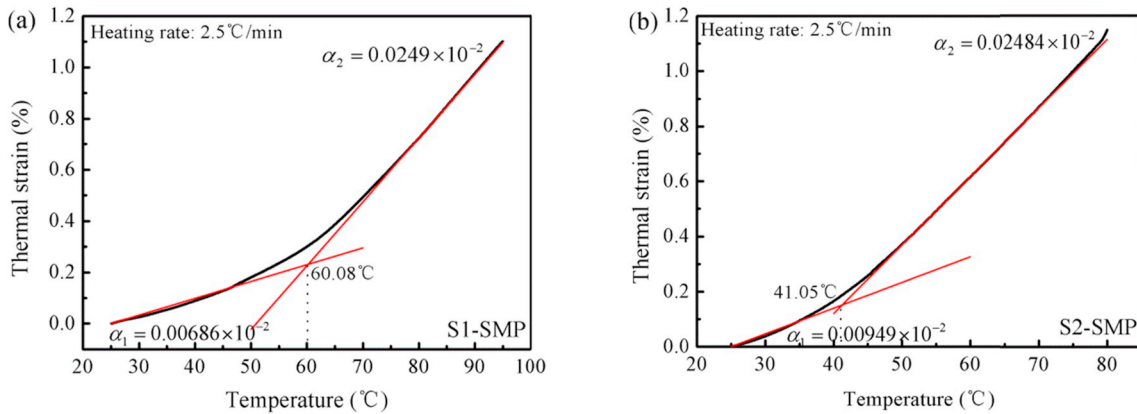


Fig. 3. Thermal expansion coefficients of S1-SMP and S2-SMP.

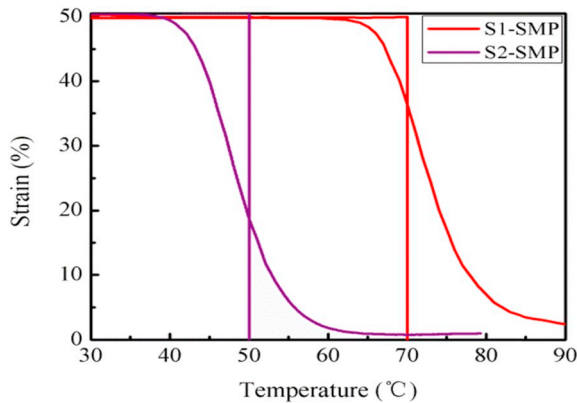


Fig. 4. Dual-SME of S1-SMP and S2-SMP.

frequency range (maybe  $10^{-5}$  Hz- $10^3$  Hz). The multi-branches relaxation modulus and relaxation time for S1-SMP and S2-SMP can be obtained by fitting the master curve under  $T_c$ . In our work, an 11-branch Generalized Maxwell model and WLF equation were applied to S1-SMP and S2-SMP respectively and the triple-SME of the segmented-SMP during a one-step temperature recovery process was demonstrated. Meanwhile, engineered implementations of triple-SME programmable self-deployed structure and smart mandrel were developed to verify the feasibility of using Generalized Maxwell models for prediction of complex movement and function.

The storage modulus distribution for the SMP over a wide frequency range can be expressed as:

$$E(f) = E_0 + \sum_{i=1}^n E_i \frac{(2\pi f)^2 \tau_i^2}{1 + (2\pi f)^2 \tau_i^2} \quad (6)$$

where,  $E_0$ ,  $n$ ,  $f$  are the moduli constant, number of branches and dynamic frequency respectively, and  $E_i$ ,  $\tau_i$  are the relaxation modulus and time for the  $i$ th branch. These parameters were different for S1-SMP and S2-SMP.

The WLF equation for the SMP is:

$$\lg \alpha_T = \frac{-C_6(T - T_c)}{C_7 + (T - T_c)} \quad (7)$$

where,  $\alpha_T$  is the shift factor,  $C_6$ ,  $C_7$  are material parameters, and  $T_c$  is a special reference temperature. These parameters were different for S1-SMP and S2-SMP.

#### 4. Results and discussion

Fig. 2 showed the results of multi-frequency scan tests of S1-SMP and S2-SMP under different isothermal condition respectively. The temperature range for the S1-SMP scans was 30 °C–100 °C and for the S2-SMP scans was 20 °C–85 °C, with intervals of 5°C used in both cases. The storage moduli of S1-SMP and S2-SMP declined monotonically with increasing temperatures.

Fig. 3 showed the relationship between thermal strain and temperature at a heating rate of 2.5 °C/min for S1-SMP and S2-SMP respectively. The results demonstrated that the thermal expansion coefficients for two SMP types were non-linear, both increasing with temperature, which could be explained by the free volume theory. Differences in the weight ratios of cross-linking agents during the synthesis process lead to different  $T_g$  values

**Table 1**  
 $R_f$  and  $R_r$  of S1-SMP and S2-SMP under uniaxial tensile test.

Materials	S1-SMP	S2-SMP
$R_f$ (%)	98.26	99.68
$R_r$ (%)	95.17	99.37

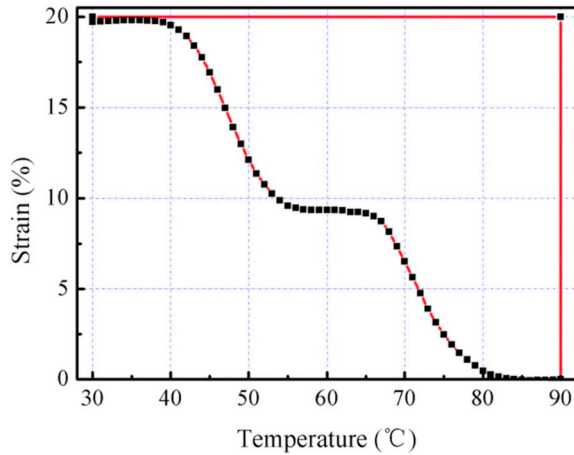


Fig. 5. Triple-SME of segmented styrene-based SMP.

for the two SMP types and it can be seen that the thermal expansion coefficients for both SMPs change when transitioning from the glass state to the rubber state. Based on the Liu model [11], the thermal strain was fitted using a second-order function, and the material parameters of the thermal expansion coefficient were found to be  $C_4 = -0.0094$ ,  $C_5 = 4.2 \times 10^{-4}$  for

S1-SMP and  $C_4 = 0.0032$ ,  $C_5 = 3.52 \times 10^{-4}$  for S2-SMP.

Fig. 4 showed the dual-shape memory behavior of the two SMP types during a typical four-step thermo-mechanical cycle. The results demonstrated that both SMPs exhibited good shape fixity ratio ( $R_f$ ) and recovery ratio ( $R_r$ ). Both ratios were higher than 95% for 50% stretching at elevated temperature, as shown in Table 1. For both SMP types the temperature at which recovery commences was in the vicinity of  $T_g$  and the glass transition zones were about 20 °C from  $T_g$ .

Fig. 5 showed the triple-shape memory behavior of the segmented-SMP with 20% stretching during a six-step thermo-mechanical cycle. During this cycle a manual process was adopted for the initial shape-programming steps (stretching and deformation). The shape recovery behavior during the sample reheating process was then characterized using the universal tensile machine. In contrast to the smooth S-shape recovery profile seen during the dual-shape recovery process, the triple-shape results demonstrated the presence of a recovery strain plateau owing to the well-separated  $T_g$  for S1-SMP and S2-SMP parts in segmented-SMP. While heating from 30 °C to 60 °C, S2-SMP part is gradually activated and S1-SMP part remained in the frozen state. Continuing heating from 60 °C to 90 °C, S2-SMP remained active and S1-SMP part gradually transitioned from frozen state to active state.

Following experimental characterization of the thermo-mechanical properties of the segmented SMP including S1-SMP and S2-SMP constituent parts, constitutive models that aimed to replicate the triple-SME behavior were proposed based on Liu model and an 11-branch Generalized Maxwell model.

Two key parameters presenting in Liu Model were determined by fitting to the experimental data for the constituent S1-SMP and S2-SMP parts. The effective elastic modulus was determined from experimental data points obtained at different temperatures, and the frozen factor was determined by fitting the free recovery strain.

For the effective elastic modulus, the material parameters based on

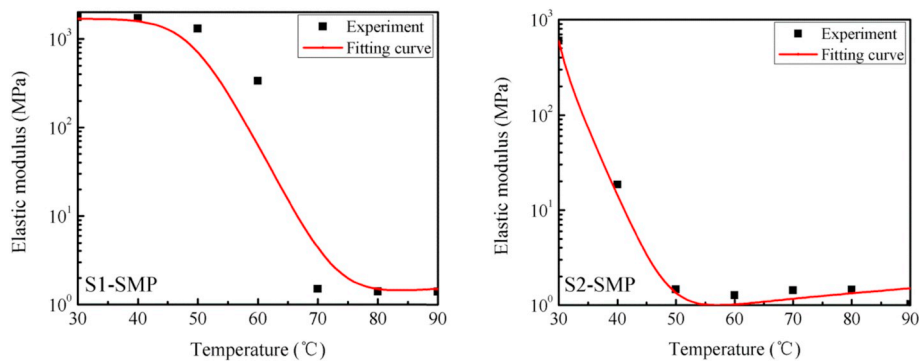


Fig. 6. Effective elastic moduli of the S1-SMP and S2-SMP parts of the segmented-SMP.

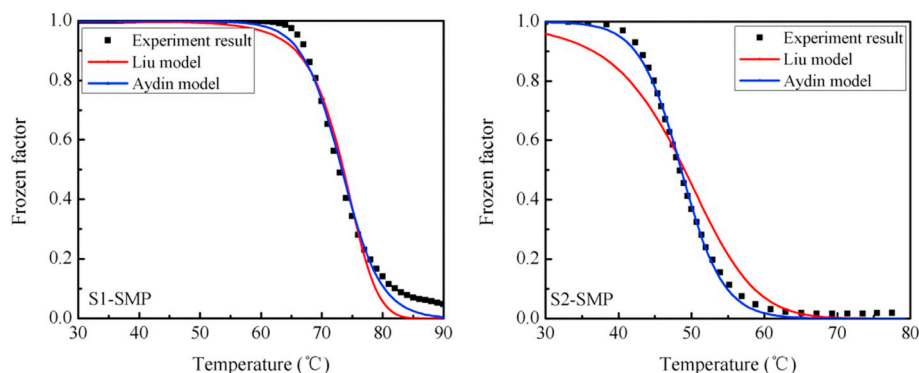


Fig. 7. Frozen factors curves of S1-SMP and S2-SMP parts in the segmented-SMP.

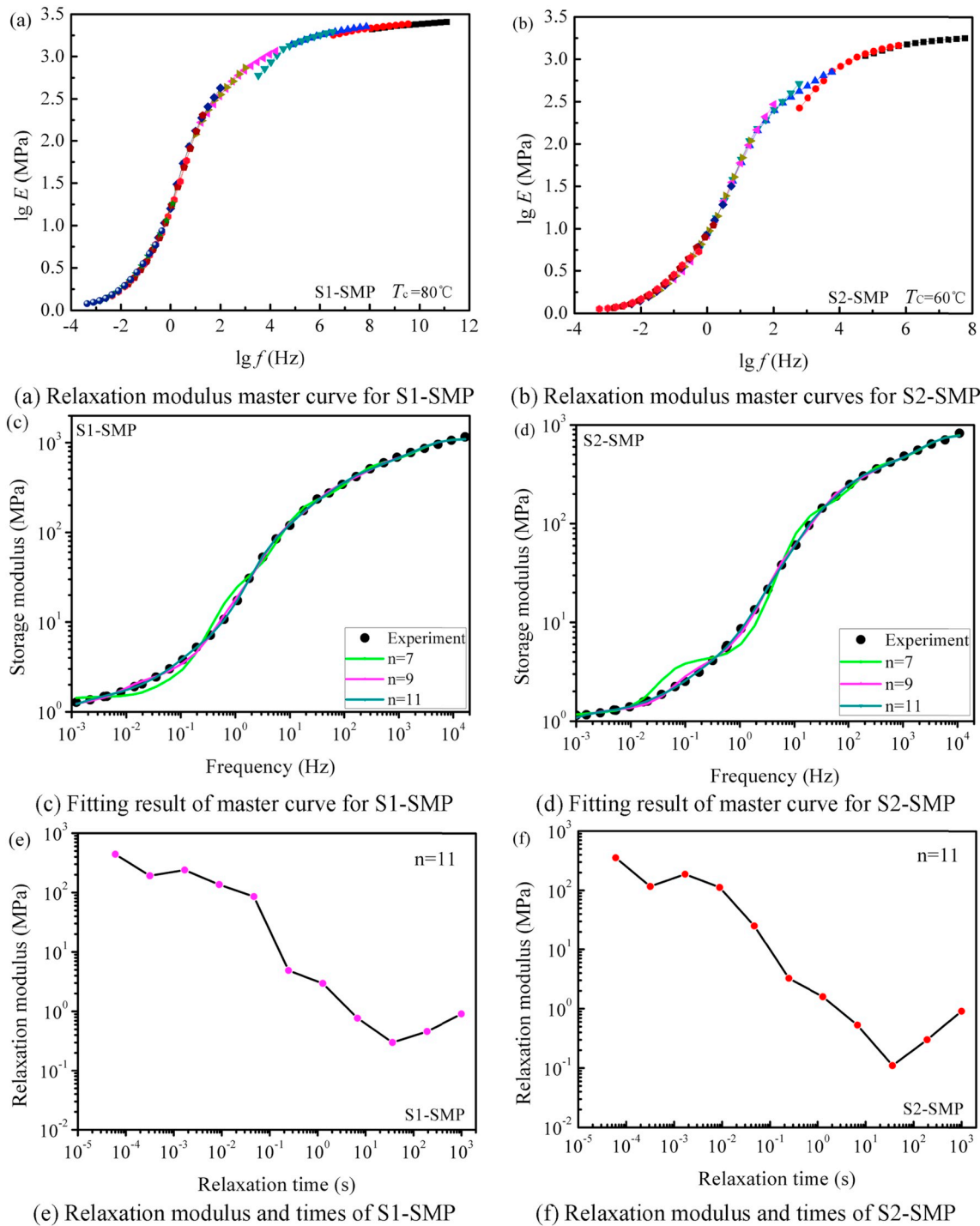


Fig. 8. Fitting of relaxation modulus master curves for the Generalized Maxwell model.

equation (1) were  $C_1 = 1700$ ,  $C_2 = 0.0167$  for S1-SMP and  $C_1 = 600$ ,  $C_2 = 0.0167$  for S2-SMP. The corresponding fitting curves are shown in Fig. 6.

For the frozen factor, two models (Liu model and Aydin model) were applied to fit the free-recovery strain data. The results demonstrated that the Aydin model offered the most effective fitting to the data for both the S1-SMP and the S2-SMP. Based on equation (3), the corresponding material parameters were  $T_r = 80^\circ\text{C}$ ,  $a = -0.0842$ ,  $b = 25.04$  for S1-SMP and  $T_r = 80^\circ\text{C}$ ,  $a = -0.3924$ ,  $b = 27.95$  for S2-SMP. The corresponding fitting curves are shown in Fig. 7. According to the established analytical forms for the effective elastic modulus and frozen factor, the

total recovery strain can then be predicted using equation (5).

Besides the Liu model, a constitutive model based on the Generalized Maxwell model was also used to understand the triple-SME behavior of the segmented SMP. Taking  $80^\circ\text{C}$  and  $60^\circ\text{C}$  as the special reference temperatures ( $T_c$ ) of S1-SMP and S2-SMP respectively, two storage modulus master curves covering the wide range frequency spectrum were obtained by shifting storage modulus curves under other temperatures, as shown in Fig. 8(a) and Fig. 8(b). The relaxation moduli and relaxation times for 7-, 9-, and 11-branch Generalized Maxwell model could be determined by fitting these two master curves based on objective function Eq. (6), as shown in Fig. 8(c) and (d). In addition, the

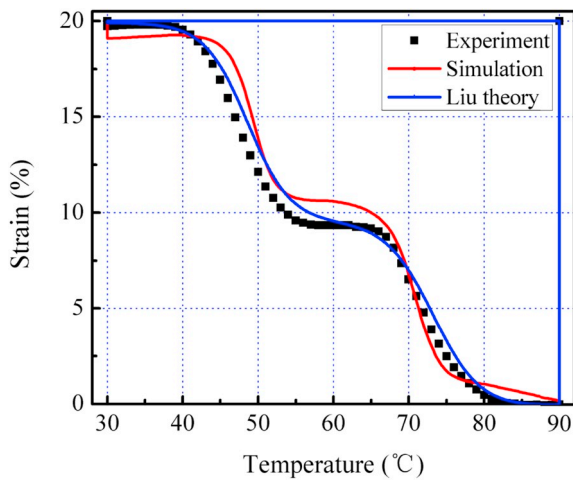


Fig. 9. Triple-shape memory model verification of the segmented styrene-based SMP.

material parameters for the WLF equations could be determined by fitting of shift factors obtained under different isothermal condition for a specified  $T_c$ . The fitting results demonstrated that 11-branch Generalized Maxwell model could better capture the trend of storage modulus under wide frequency range, the corresponding relaxation modulus and times could be seen in Fig. 8(e) and (f), in which the  $E_0$  could be seen elastic modulus of SMP under high temperature and Poisson ratio was 0.4. Once these material parameters were obtained, the finite element software ABAQUS 6.12 was applied to simulate the shape memory process of triple-SME in the segmented SMP.

Experimental triple-SME data for the segmented styrene-based SMP, in which the S1-SMP and S2-SMP regions were individually placed

under 20% tension strain, was compared with the predicted results from the Liu model and the Generalized Maxwell model, respectively, as shown in Fig. 9. The model predictions were in good agreement with observed SMP recovery profile. Such models can therefore provide a theoretical basis for the understanding of triple-SME of segmented-SMPs under uniaxial deformation. Moreover, simulations based on Generalized Maxwell model were also used to study triple-SME behavior of complex three-dimensional structures.

### 5. Applications of SMP with triple-SME

#### 5.1. Programmable self-deployed structure

SMP plates made from the two types of SMP materials (S1-SMP and S2-SMP) were cut into rectangular strips with dimensions 60 mm × 10 mm × 2.8 mm (length × width × thickness). These samples were then assembled into a self-deployed structure with an initial 2D flat state, in which SMPs with identical material properties were aligned in the same direction, as shown in Fig. 10(a). The self-deployed structure was then heated to a high temperature  $T_H$  ( $T_H \geq T_{g1} + 20^\circ\text{C}$ )

Table 2

Temperature condition of self-deployed structure for shape memory process.

Step	Time	Deformation behavior
1	0–1 S	Heating to temperature 90°C and blending SMP plates to 145°
2	1–721 S	Keeping blend angle and cooling to 60 °C to freeze S1-SMPs
3	721–1441 S	Keeping blend angle and continue cooling to 30 °C to freeze S2-SMPs
4	1441–1442 S	Temperature 30 °C and removing external load
5	1442–2162 S	Reheating to 60 °C and S2-SMPs recover initial shape
6	2162–2882 S	Continuing heating to 90 °C and S1-SMPs recover initial shape

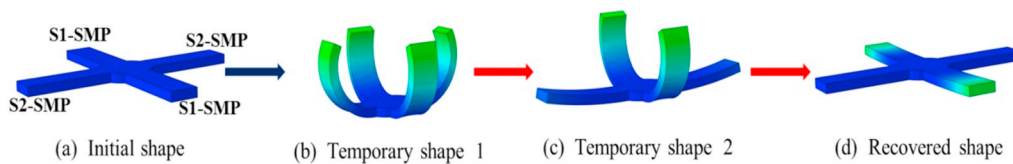


Fig. 10. Schematic of triple-shape memory process for self-deployed structure.

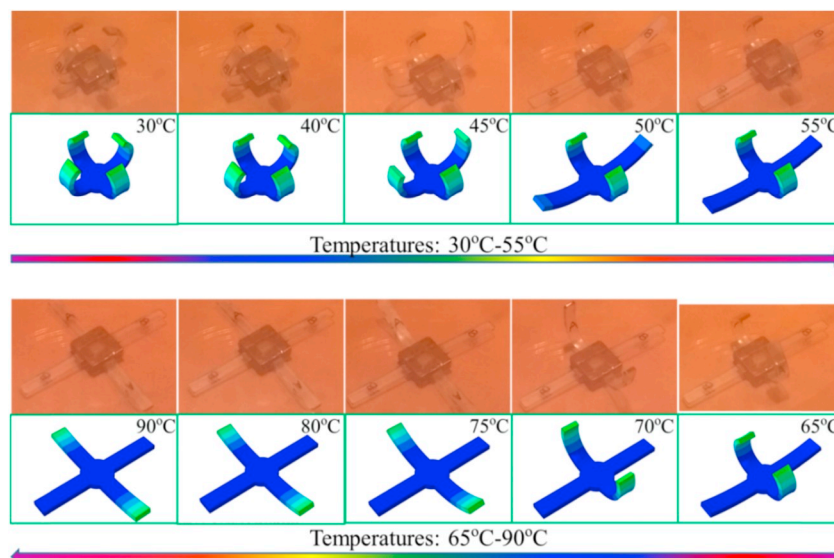


Fig. 11. Sequential shape recovery of self-deployed structure.

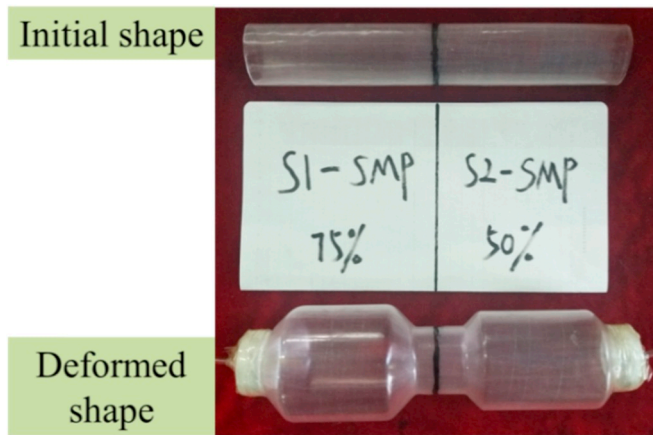


Fig. 12. Initial and deformed shapes of double bottle-shaped SMP mandrel.

and bent into a 3D folded “flower” state with a bending angle of  $145^\circ$ . The deformation was then held while the temperature was reduced to a low temperature  $T_L$  ( $T_L < T_{g2}$ ), and after removing the bending load and allowing for a little mechanical spring-back, temporary shape 1 was obtained as shown in Fig. 10(b). Following reheating to a middle temperature  $T_M$  ( $T_{g1} > T_M > T_{g2}$ ), the S2-SMP samples with lower  $T_g$  almost fully recovered the initial flat state and the S1-SMP samples maintained the deformation of temporary shape 1, such that the folded “flower” was partly deployed, as shown in Fig. 10(c). Continuing heating to the high temperature  $T_H$  ( $T_H \geq T_{g1} + 20^\circ\text{C}$ ), the S1-SMP samples also returned to the initial 2D flat state and the folded “flower” was completely deployed, as shown in Fig. 10(d). It was interesting to observe how a “flower” with petals made of different SMPs could be used as an ambient temperature sensor in which petal pairs with different  $T_g$ s would progressively deploy and “bloom” as the temperature increased.

Fig. 11 demonstrated the shape recovery process of the self-deployed structure as the temperature was progressively increased up to  $T_H$ .  $T_L$ ,  $T_M$  and  $T_H$  were selected as  $30^\circ\text{C}$ ,  $60^\circ\text{C}$  and  $90^\circ\text{C}$ , respectively, and the heating rate was  $2.5^\circ\text{C}/\text{min}$ , there was good agreement with FEM simulation results. The element type was hybrid, incompatible element for two types of SMP plates. One end of SMP plates connecting to base were fixed, the other end was free to blend. The detailed temperature condition during shape memory process was shown in Table 2.

When temperature was increased to  $40^\circ\text{C}$  during recovery step, still lower than  $T_{g2}$  ( $43^\circ\text{C}$ ), there was little change with the entire structure remaining in the frozen state and holding temporary shape 1. Continuing to  $45^\circ\text{C}$ , the S2-SMP segments gradually entered the transition zone and recover temporary shape 2. At  $55^\circ\text{C}$ , still below  $T_{g1}$  ( $62^\circ\text{C}$ ), recovery of temporary shape 2 was complete; the S2-SMP segments reached the rubber state and essentially recovered their initial 2D flat state, but the S1-SMP segments remained in the frozen state. Continuing to  $65^\circ\text{C}$ , there was little change for the S1-SMP segments with only slight recovery, but between  $65^\circ\text{C}$  and  $80^\circ\text{C}$ , the S1-SMP segments progressively recovered its initial shape, until at  $80^\circ\text{C}$ , the entire structure reached the rubber state. Continuing to  $90^\circ\text{C}$ , the residual strain was slowly recovered and the original 2D flat state was almost fully restored. It was noted that there is incomplete recovery of residual strain when heating to  $T_M/T_H$  due to the viscoelastic properties of SMP materials, but this imperfection can be largely eliminated by increasing the holding time at high temperature. In addition, it was observed that the self-deployed structure showed few signs of shape recovery when the temperature was less than the  $T_g$  of the SMP materials, but that shape recovery was nearly complete  $10^\circ\text{C}$ - $20^\circ\text{C}$  above  $T_g$ .

## 5.2. Triple-shape memory smart mandrel

Owing to low-cost, simple fabrication process, and high shape deformation and recovery characteristics, SMP mandrels with a single temporary shape have been investigated as a means to fabricate composite structures with complex surfaces [49,50]. Everhart et al. from Cornerstone Research Group Inc. (CRG) fabricated a single bottle-shaped SMP mandrel using an inflation method [49]. In this work, a triple-SME segmented SMP tube made from S1-SMP and S2-SMP was prepared using the two-step curing method and its deformation behavior was investigated in the context of a smart mandrel. The initial tubular form was used as the initial shape of the triple-SME mandrel. The tube was then inflated into a double bottle-shaped form at high temperature ( $90^\circ\text{C}$ ) with the aid of an external rigid mold. This deformed shape was largely retained after cooling to room temperature and removal of the inflating load. The initial and deformed shapes of the triple-SME smart mandrel are shown in Fig. 12. The S1-SMP and S2-SMP segments of the mandrel were subjected to 75% and 50% deformation in the radial direction respectively.

Owing to the well-separated  $T_g$ s of the two constituent SMP

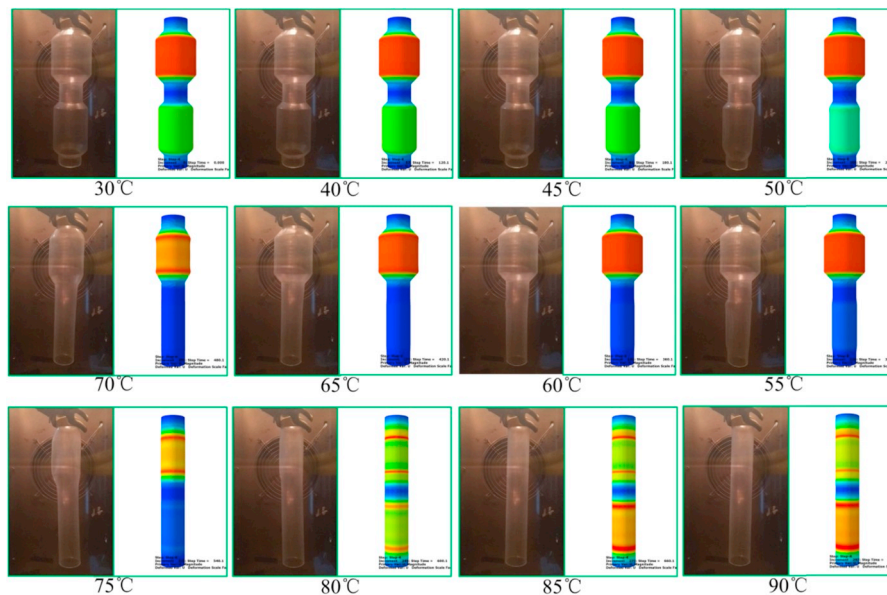


Fig. 13. Sequential shape recovery of double bottle-shaped SMP mandrel.

materials, the double bottle-shaped mandrel was able to remember two temporary shapes. Fig. 13 records the individual shape recovery process of the S1-SMP and S2-SMP segments at a heating rate of 5 °C/min. Similar with above-mentioned self-deployed structure, FEM simulations based on the Generalized Maxwell model were able to provide an indicative prediction of the sequential shape recovery behavior with triple-SME for smart mandrel. The element was hybrid, incompatible element for SMP tube. The two ends of tube were fixed and the interface of S1-SMP and S2-SMP at the center part of tube was hindered axial movement. The detailed temperature condition during shape memory process was same with self-deployed structure expect the rate was 5 °C/min. The good agreement was showed by using both FEM simulation and experimental observation during total recovery process, a little more quickly recovery in FEM was due to fitting errors for SMP material parameters. At temperatures up to 45 °C, the S2-SMP segment largely retained the deformed shape with only very slight recovery. Continuing heating to 60 °C, the S2-SMP segment almost completely recovered the initial tube state while the S1-SMP segment retained its deformation. At 65 °C, the S1-SMP segment showed slight recovery and continued heating to 80 °C allowed the entire structure to almost fully return to the initial tube state. At the terminal temperature of 90 °C, the residual deformation of the smart mandrel was also almost fully recovered.

## 6. Conclusions

In this paper, a segmented styrene-based triple-SMP comprising S1-SMP and S2-SMP with well-separated  $T_g$  (62 °C and 43 °C) was prepared. Multi-frequency scan testing, thermal expansion measurements, static tensile testing and shape memory testing were conducted to characterize the thermo-mechanical properties of the S1-SMP and S2-SMP materials. Four-step thermo-mechanical cycle testing demonstrated the dual-shape memory behavior, with high shape fixity and shape recovery ratios in excess of 95%. The triple-SMP prepared from these two constituent materials exhibited the expected triple-SME shape recovery effect over the range 30 °C–90 °C. Furthermore, triple shape recovery behavior under uniaxial tensile strain of 20% was in good agreement with the predictions of constitutive models based on the Liu and Generalized Maxwell models. Finally, triple-SME behavior was demonstrated in two engineered implementations: a programmable self-deployed structure and a double bottle-shaped smart mandrel. In both cases experimental shape recovery data were in good agreement with the predictions of FEM simulations.

## Acknowledgments

This work is supported by the National Natural Science Foundation of China: Grant No. 11632005, 11672086.

## References

- Leng JS, Lan X, Liu YJ, Du SY. Shape memory polymers and their composites: stimulus methods and applications. *Prog Mater Sci* 2011;56(7):1077–135.
- Meng H, Li GQ. A review of stimuli-responsive shape memory polymer composites. *Polymer* 2013;6(3):738–81.
- Sun L, Huang WM, Ding Z, Zhao Y, Wang CC, Purnawali H, Tang C. Stimulus-responsive shape memory materials: a review. *Mater Des* 2012;33:577–640.
- Hager MD, Bode S, Weber C, Schubert US. Shape memory polymers: past, present and future developments. *Prog Polym Sci* 2015;49–50:3–33.
- Behl M, Lendlein A. Shape memory polymers. *Mater Today* 2007;10(4):20–8.
- Hu JL, Zhu Y, Huang HH, Lu J. Recent advances in shape memory polymers: structure, mechanism, functionality and modeling and applications. *Prog Polym Sci* 2012;37(12):1720–63.
- Xie F, Huang LN, Leng JS, Liu YJ. Thermoset shape memory polymers and their composites. *J Intell Mater Syst Struct* 2016;27(18):2433–55.
- Wagermaier W, Kratz K, Heuchel M, Lendlein A. Characterization methods for shape memory polymers. *Advanced in Polymer Science* 2009;226:97–145.
- Liu TZ, Zhou TY, Yao YT, Zhang FH, Liu LW, Liu YJ, Leng JS. Stimulus methods of multi-functional shape memory polymer nanocomposites: a review. *Compos Appl Sci Manuf* 2017;100:20–30.
- Tobushi H, Hara H, Yamada E, Hayashi S. Thermomechanical constitutive modeling in shape memory polymer of polyurethane series. *J Intell Mater Syst Struct* 1997;8(8):717–8.
- Liu YP. Thermomechanical behavior of shape memory polymers. University of Colorado; 2004.
- Qi HJ, Nguyen TD, Castroa F, Yakacki CM, ShandaSa R. Finite deformation thermo-mechanical behavior of thermally induced shape memory polymers. *J Mech Phys Solids* 2008;56(5):1730–51.
- Liu YJ, Du HY, Liu LW, Leng JS. Shape memory polymers and their composites in aerospace applications: a review. *Smart Mater Struct* 2014;23(2):023001.
- Lendlein A, Behl M, Hiebl B, Wischke C. Shape memory polymers as a technology platform for biomedical applications. *Expert Rev Med Devices* 2010;7(3):357–79.
- Hu JL, Meng HP, Li GQ, Ibeke SI. A review of stimuli-responsive polymers for smart textile applications. *Smart Mater Struct* 2012;21(5):053001.
- Prersch T, Ecker M, Schildhauer M, Maskos M. Switchable information carriers based on shape memory polymer. *J Mater Chem* 2012;22(16):7757–66.
- Takashima K, Rossiter J, Mukai T. McKibben artificial muscle using shape memory polymer. *Sensor Actuator Phys* 2010;164(1–2):116–24.
- Bellini Kelch S, Langer R, Lendlein A. Polymeric triple-shape materials. *Proc Natl Acad Sci USA* 2006;103(48):18043–7.
- Behl M, Lendlein A. Triple-shape polymers. *J Mater Chem* 2010;20(17):3335–45.
- Pretsch T. Triple-shape properties of a thermoresponsive poly(ester urethane). *Smart Mater Struct* 2010;19(1):015006.
- Pretsch T. Durability of a polymer with triple-shape properties. *Polym Degrad Stab* 2010;95(12):2515–24.
- Chen SJ, Hu JL, Yuen CWM, Chan LK, Zhuo HT. Triple shape memory effect in multiple crystalline polyurethanes. *Polym Adv Technol* 2010;21(5):377–80.
- Xia L, Wang Y, Lu N, Xin ZX. Facile fabrication of shape memory composites from natural eucommia rubber and high density polyethylene. *Polym Int* 2017;66(5):653–8.
- Xie T, Rousseau IA. Facile tailoring of thermal transition temperatures of epoxy shape memory polymers. *Polymer* 2009;50(8):1852–6.
- Xie T, Xiao XC, Cheng YT. Revealing triple-shape memory effect by polymer bilayers. *Macromol Rapid Commun* 2009;30(21):1823–7.
- Bae CY, Park JH, Kim EY, Kang YS, Kim BK. Organic-inorganic nanocomposite bilayers with triple shape memory effect. *J Mater Chem* 2011;21(30):11288–95.
- Podgorski M, Wang C, Bowman CN. Multiple shape memory polymers based on laminates formed from thiol-click chemistry based polymerizations. *Soft Matter* 2015;11(34):6852–8.
- Yang B, Huang WM, Li C, Lee CM, Li L. On the effect of moisture in a polyurethane shape memory polymer. *Smart Mater Struct* 2004;13(1):191–5.
- Huang WM, Yang B, An L, Li C, Chan YS. Water-driven programmable polyurethane shape memory polymer: demonstration and mechanism. *Appl Phys Lett* 2005;86(11):114105.
- Wang L, Yang XF, Chen HM, Yang G, Gong T, Li WB, Zhou SB. Multi-stimuli sensitive shape memory poly(vinyl alcohol)-graft-polyurethane. *Polym Chem* 2013;4(16):4461–8.
- Xie T. Tunable polymer multi-shape memory effect. *Nature* 2010;464(7286):267–70.
- Li JJ, Xie T. Significant impact of thermo-mechanical conditions on polymer triple-shape memory effect. *Macromolecules* 2011;44(1):175–80.
- Zhang FH, Zhang ZC, Liu YJ, Lv HB, Leng JS. The quintuple-shape memory effect in electrospun nanofiber membranes. *Smart Mater Struct* 2013;22(8):085020.
- Zhang QW, Wei HQ, Liu LW, Leng JS, Du SY. Triple-shape memory effects of bismaleimide based thermosetting polymer networks prepared via heterogeneous crosslinking structures. *RSC Adv* 2016;6(13):10233–41.
- Yang ZH, Chen Y, Wang QH, Wang TM. High performance multiple-shape memory behaviors of poly(benzoxazole-co-imide)s. *Polymer* 2016;88:19–28.
- Kumar UN, Kratz K, Wagermaier W, Behl M, Lendlein A. Non-contact actuation of triple-shape effect in multiphase polymer network nanocomposites in alternating magnetic field. *J Mater Chem* 2010;20(17):3404–15.
- He ZW, Satarkar N, Xie T, Cheng YT, Hilt JZ. Remote controlled multishapepolymer nanocompositeswith selective radiofrequency actuations. *Adv Mater* 2011;23(28):3192–6.
- Li WB, Liu YJ, Leng JS. Selectively actuated multi-shape memory effect of a polymer multicomposite. *J Mater Chem* 2015;3(48):24532–9.
- Wu Y, Hu JL, Zhang C, Han J, Wang Y, Kumar B. A facile approach to fabricate a UV/heat dual-responsive triple shape memory polymer. *J Mater Chem* 2015;3(1):97–100.
- Yu L, Wang Q, Sun J, Li CY, Zou C, He ZM, Wang ZD, Zhou L, Zhang LY, Yang H. Multi-shape-memory effects in a wavelength-selective multicomposite. *J Mater Chem* 2015;3(26):13953–61.
- Sun L, Huang WM. Mechanisms of the multi-shape memory effect and temperature memory effect in shape memory polymers. *Soft Matter* 2010;6(18):4403–6.
- Yu K, Xie T, Leng JS, Ding YF, Qi HJ. Mechanisms of multi-shape memory effects and associated energy release in shape memory polymers. *Soft Matter* 2012;8(20):5687–95.
- Arrieta S, Diani J, Gilormini P. Experimental characterization and thermoviscoelastic modeling of strain and stress recoveries of an amorphous polymer network. *Mech Mater* 2014;68:95–103.
- Zhang DW, Liu YJ, Yu K, Leng JS. Influence of cross-linking agent on thermomechanical properties and shape memory effect of styrene shape memory polymer. *J Intell Mater Syst Struct* 2011;22(18):2147–54.
- Du HY, Liu LW, Zhang FH, Zhao W, Leng JS, Liu YJ. Thermal-mechanical behavior of styrene-based shape memory polymer tubes. *Polym Test* 2017;57:119–25.

- [46] Du HY, Liu LW, Zhang FH, Leng JS, Liu YJ. Shape retainability and reusability investigation of bottle-shaped SMP mandrel. *Polym Test* 2018;69:325–31.
- [47] Rasa KM, Steeb H, Aydin AO. On the evolution law for the frozen fraction in linear theories of shape memory polymers. *Arch Appl Mech* 2012;82(8):1103–15.
- [48] Yu K, Qi HJ. Temperature memory effect in amorphous shape memory polymers. *Soft Matter* 2014;10(47):9423–32.
- [49] Everhart MC, Stahl J. Reusable shape memory polymer mandrels. *Proc SPIE* 2005; 5762:27–34.
- [50] Zhang L, Du HY, Liu LW, Liu YJ, Leng JS. Analysis and design of smart mandrels using shape memory polymers. *Compos B Eng* 2014;59:230–7.